Smart Grid and Renewable Energy, 2025, 16(8), 147-176
https://www.scirp.org/journal/sgre
ISSN Online: 2151-4844
ISSN Print: 2151-481X

Intelligent System for Voltage Fault Detection in Electrical Networks: A Neuro-Fuzzy Approach with Hybrid Transmission (Fiber, 4G, VSAT)

Nianga-Apila[1], Rodolphe Gomba[1], Anedi Oko Ganongo[1], Mathurin Gogom[1], Gilbert Ganga[1], Amos Omboua Eyandzi[1], Tite Lawd Ngouloubi[1], Rozan Etoua Ndouniama[2]

[1]Polytechnic Superior National School (ENSP), Marien Ngouabi University, Brazzaville, Congo
[2]Faculty of Letters, Arts and Human Sciences (FLASH), Marien Ngouabi University, Brazzaville, Congo
Email: apilanianga@gmail.com

How to cite this paper: Nianga-Apila, Gomba, R., Oko Ganongo, A., Gogom, M., Ganga, G., Omboua Eyandzi, A., Ngouloubi, T.L. and Etoua Ndouniama, R. (2025) Intelligent System for Voltage Fault Detection in Electrical Networks: A Neuro-Fuzzy Approach with Hybrid Transmission (Fiber, 4G, VSAT). *Smart Grid and Renewable Energy*, **16**, 147-176.
https://doi.org/10.4236/sgre.2025.168009

Received: August 2, 2025
Accepted: October 19, 2025
Published: October 22, 2025

Abstract

The reliability of the power supply depends heavily on the ability of operators to quickly detect and classify voltage disturbances. In the context of Congo-Brazzaville, structural limitations in communication infrastructure make this challenge particularly complex. This article proposes an innovative approach combining an ANFIS neuro-fuzzy system with a hybrid remote transmission architecture combining fiber optics, 4G/LTE, and VSAT. The model is based on the joint integration of electrical indices (RMS values, symmetrical components, THD) and network quality of service metrics (latency, jitter, losses) into fuzzy premises, in order to strengthen decision-making robustness in the face of heterogeneous transmission conditions. MATLAB/Simulink simulations demonstrate that ANFIS significantly outperforms conventional RMS threshold and ANN approaches: classification accuracy reaches 97.8% over fiber and remains at 94.3% over 4G and 88.6% over VSAT, with a median detection delay reduced to 12 ms over fiber and 41 ms over 4G. This performance complies with regulatory recommendations (EN 50160, IEC 61000-4-30) and confirms the value of near real-time deployment. Beyond the experimental results, the study paves the way for the modernization of African electrical grids by combining artificial intelligence and communications resilience. It establishes a credible scientific basis for the implementation of Smart Grid solutions adapted to constrained environments.

Keywords

ANFIS, Hybrid Data Transmission, Sag, Swell, Power Quality, Smart Grid, Fibre Optics, 4G/LTE, VSAT, MATLAB/Simulink, Fault Diagnosis, High-Voltage Networks, QoS-Aware Monitoring

1. Introduction

The quality of electrical energy is now a major challenge for transmission and distribution networks, particularly in developing countries where continuity of service directly affects economic and social stability. Among the most common and damaging disturbances are voltage sags and swells. These transient phenomena, caused by short circuits, switching operations, or load imbalances, lead to unexpected shutdowns of industrial equipment, production losses, and accelerated degradation of sensitive equipment. In a context where critical infrastructure is heavily dependent on electricity (hospitals, telecommunications, extractive industries), the economic and operational impact of sags and swells is considerable [1]-[3].

In Central Africa, and more specifically in Congo-Brazzaville, the high-voltage electricity grid has several structural characteristics that increase its vulnerability to these disruptions. On the one hand, the topology of the grid, characterized by long lines with high exposure to the elements, promotes the occurrence of transient and permanent faults. On the other hand, regional disparities in fiber optic or cellular network coverage make it difficult to implement reliable real-time monitoring systems. These constraints limit the effectiveness of traditional monitoring solutions, which are generally designed for interconnected and densely equipped networks such as those in Europe or North America [4]-[7].

Traditional approaches to disturbance detection based on fixed thresholds, root mean square (RMS) calculations, or spectral transforms are not well suited to Congolese environments. Their sensitivity to noise, inability to capture rapid variations, and lack of intelligent classification mechanisms reduce their relevance. Furthermore, these methods often assume stable and consistent data transmission, which is far from guaranteed in a context of heterogeneous connectivity [8]-[10].

Given these limitations, artificial intelligence systems, and in particular ANFIS (Adaptive Neuro-Fuzzy Inference System) models, offer a robust alternative. ANFIS combines the learning capacity of neural networks with the linguistic representation flexibility of fuzzy logic, enabling accurate and uncertainty-tolerant detection, classification, and characterization of disturbances. However, the effectiveness of this diagnosis depends on the continuous availability of reliable data, which requires a resilient communication architecture [4] [11]-[13].

It is with this in mind that the adoption of an adaptive hybrid transmission system integrating fiber optics, 4G/LTE, and VSAT is essential. This architecture allows us to take advantage of the complementary strengths of these technologies: low latency fiber for urban areas, flexible 4G for suburban areas, and universal VSAT coverage for remote regions. By dynamically prioritizing flows according to their criticality and automatically switching over in the event of failure, this hybridization ensures continuity of monitoring and robustness of ANFIS diagnostics [14]-[19].

In this paper, we propose a comprehensive methodology for the intelligent detection of voltage dips and surges in the Congolese high-voltage network, based on the integration of an ANFIS model and a hybrid communication architecture.

The main contributions of this article are as follows:

- the development of a synoptic pipeline linking field measurement, hybrid transmission, and ANFIS diagnostics;
- the implementation of an adaptive routing and automatic failover mechanism to secure critical flows in heterogeneous environments;
- Modeling and simulation in MATLAB/Simulink of the transmission chain and ANFIS diagnostics, validating the accuracy and robustness of the approach;
- the study's focus on the real-life case of Congo-Brazzaville, offering an applied and contextualized scientific contribution to the challenges facing African networks.

This original combination of neuro-fuzzy intelligence and hybrid transmission paves the way for more reliable and intelligent supervision of high-voltage networks in Africa, and is an important milestone towards the implementation of resilient Smart Grids in constrained environments.

2. Literature Review

2.1. Voltage Disturbances in High-Voltage Networks

Voltage fluctuations mainly occur in the form of sags and swells. Here, we formally link the time model of the signal to the sliding effective value and the normative classification criteria. We model the voltage of a phase using a slow envelope sinusoid:

$$v(t)=\sqrt{2}V_{\text{nom}}\left(1+\delta(t)\right)\sin(\omega t), \tag{1}$$

where V_{nom} is the *nominal RMS voltage* (50 Hz in Congo, $\omega=2\pi f$) and $\delta(t)$ describes the relative (dimensionless) deviation of the amplitude from the nominal value. Thus, $\delta(t)=0$ corresponds to normal conditions; $\delta(t)<0$ indicates a decrease in amplitude (sag) and $\delta(t)>0$ indicates an increase (swell). The sliding effective value is defined by

$$V_{\text{rms}}(t)=\sqrt{\frac{1}{T}\int_{t}^{t+T}v^{2}(\tau)\,\mathrm{d}\tau},\quad T=\frac{2\pi}{\omega}. \tag{2}$$

We introduce the quantity *pu* $u(t)=V_{\text{rms}}(t)/V_{\text{nom}}$. By setting

$$S_{1}(t)=\frac{2}{T}\int_{t}^{t+T}\delta(\tau)\sin^{2}(\omega\tau)\,\mathrm{d}\tau,\quad S_{2}(t)=\frac{2}{T}\int_{t}^{t+T}\delta^{2}(\tau)\sin^{2}(\omega\tau)\,\mathrm{d}\tau \tag{3}$$

we have the identity

$$u^{2}(t)=1+2S_{1}(t)+S_{2}(t). \tag{4}$$

If the envelope is **quasi-stationary over a period** ($\delta(\tau)\approx\delta(t)$ for $\tau\in[t,t+T]$), then

$$u(t)=\left|1+\delta(t)\right|\approx 1+\delta(t)\ \left(\text{pour}\ |\delta|\ll 1\right), \tag{5}$$

In the first order (minor deviations), we obtain the linear approximation

$$u(t)\approx 1+S_{1}(t), \tag{6}$$

that is, $u(t)$ is governed by the weighted average of δ over the window, weighted by $\sin^2$. The normative criteria are naturally expressed in pu via $u(t)=V_{\text{rms}}(t)/V_{\text{nom}}$:

$$\text{sag}: u(t)\in[0.1,0.9] \text{ over an interval } \Delta t\in[0.5T, \text{a few seconds}], \tag{7}$$

$$\text{swell}: u(t)\in[1.1,1.8] \text{ on the same type of interval.} \tag{8}$$

Under the quasi-stationary assumption (5), these conditions can be rewritten (approximately) in terms of relative deviation:

$$\text{sag} \Leftrightarrow \delta(t)\in[-0.9,-0.1],\ \text{swell} \Leftrightarrow \delta(t)\in[+0.1,+0.8]. \tag{9}$$

In the first order (6), the decision depends on the weighted average $S_1(t)$, which justifies the use of a half-period *moving RMS* to track the evolution of $u(t)$. The entry/exit times $(t_{\text{in}}, t_{\text{out}})$ are defined as the first times at which $u(t)$ crosses the thresholds of (7) (8) in a sliding window; the duration is $\Delta t = t_{\text{out}} - t_{\text{in}}$. For robustness in the presence of noise, hysteresis thresholds $u_{\downarrow} < 0.9 < u_{\uparrow}$ (resp. $1.1 < u_{\downarrow}^{+} < u_{\uparrow}^{+} < 1.8$) are introduced.

In order to avoid decision oscillations. Equation (4) shows that classification depends on a local average of the amplitude deviation; long, weakly redundant HT lines (Congolese case) favor sequences $\delta(t)$ that are consistent over several periods, making (5) applicable and detection reliable, provided that updates are made at half-period intervals and noise filtering is applied.

2.2. Conventional Detection Methods and Their Limitations

Traditional approaches are mainly based on: sliding RMS thresholds, spectral estimation (DFT/FFT) of the fundamental frequency, and time-scale analysis (wavelets). Their principles are outlined below, and explicit decision rules and their intrinsic limitations in the context of African/Congolese high-voltage networks (heterogeneous infrastructure, measurement noise, intermittent transmission) are derived from them [8]-[10].

2.2.1. Sliding RMS Thresholds

A signal is observed

$$v[n] = V_{\text{nom}}\left(1+\delta[n]\right)\sin\left(\omega_0 n T_s + \phi\right) + \eta[n], \tag{10}$$

where $|\delta[n]|$ measures the amplitude deviation (drop/surge), $\eta[n]$ is additive noise (zero-mean, variance σ^2). Over a window of N samples, the RMS estimator is

$$\hat{V}_{\text{rms}}[k] = \sqrt{\frac{1}{N}\sum_{n=k-N+1}^{k} v^2[n]}. \tag{11}$$

For a 50 Hz network, a relative threshold τ (e.g., $\tau = 0.10$) and a minimum duration Δt (e.g., ≥ half-period) are set. The simple rule is

$$\frac{\left|\hat{V}_{\text{rms}}[k] - V_{\text{nom}}\right|}{V_{\text{nom}}} > \tau \text{ during } \geq \Delta t. \tag{12}$$

If $\delta[n] \equiv \delta$ is constant over the window and $\eta[n]$ is negligible,

$$\mathbb{E}\left[\hat{V}_{\text{rms}}\right] \approx V_{\text{nom}}\left|1+\delta\right|. \tag{13}$$

Thus, a decrease of 20% ($\delta = -0,2$) shifts the estimate by approximately −20%. Noting that $\hat{P} = \frac{1}{N}\sum v^2[n]$, we have (approx.) $\text{Var}\left(\hat{P}\right) \approx \frac{1}{N}\text{Var}\left(v^2\right)$; under pure sine plus white noise, $\hat{V}_{\text{rms}} = \sqrt{\hat{P}}$ and, by the delta method

$$\text{Var}\left(\hat{V}_{\text{rms}}\right) \approx \frac{\text{Var}\left(\hat{P}\right)}{4P}, \quad P = V_{\text{nom}}^2 + \sigma^2. \tag{14}$$

The absolute threshold $T = \tau V_{\text{nom}}/\sqrt{2}$ gives

$$\text{PFA} \approx Q\left(\frac{T}{\sqrt{\text{Var}\left(\hat{V}_{\text{rms}}\right)}}\right), \tag{15}$$

where $Q(\cdot)$ is the Gaussian tail function. Therefore, for a given noise level σ, longer windows (large N) are required to maintain the FAL (false alarm rate under noise), at the cost of a minimum detection delay $\geq (N-1)T_s$. This strategy suffers from a detection delay linked to the window, high sensitivity to impulse noise and brief dips, ambiguities with inrush/switching, and fixed thresholds that are not very robust to slow drifts in V_{nom}. **Figure 1** shows the evolution of the moving average over a time window T, sampled at intervals of $T/2$.

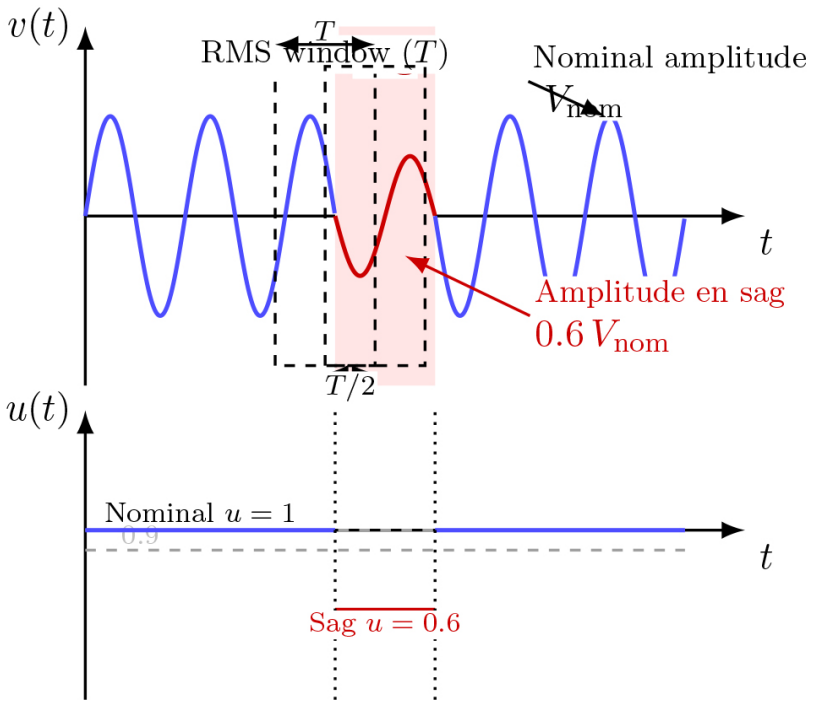

Figure 1. Moving average value over a period (*T*) with a step size of *T*/2.

2.2.2. Frequency Estimation (DFT/FFT) of the Fundamental

The fundamental complex amplitude is estimated by the DFT on N points:

$$\hat{A}_1 = \frac{2}{N}\sum_{n=0}^{N-1} v[n]\mathrm{e}^{-j2\pi n/N}. \tag{16}$$

Detecting a drop/surge is equivalent to testing.

$$\left|\hat{A}_1\right| \lessgtr (1 \mp \tau)V_{\text{nom}}. \tag{17}$$

If the actual frequency is $f_0 + \Delta f$ (slip), the modulus is attenuated by the spectral leakage via the Dirichlet kernel:

$$\hat{A}_1 \approx A_1 \frac{\sin(\pi N\epsilon)}{N\sin(\pi\epsilon)}\mathrm{e}^{j\varphi},\ \epsilon = \frac{\Delta f}{f_s}. \tag{18}$$

So even without defects, a slight Δf (common in Central Africa, where speed regulation can fluctuate) biases $\left|\hat{A}_1\right|$ and causes false detections. Furthermore, an amplitude discontinuity in the window amounts to convolving the spectrum by the TF of the window (side lobes) $\Rightarrow$ **overestimations** or **underestimations** during transients. This approach requires an integer number of periods or apodized windows (leakage/bias compromise), remains sensitive to frequency fluctuations and harmonics, and induces a delay at least equal to the window.

2.2.3. Wavelet Analysis (DWT/CWT)

The CWT of $v(t)$ by a mother wavelet ψ is

$$W_v(a,b) = \frac{1}{\sqrt{|a|}}\int_{\mathbb{R}} v(t)\psi^*\left(\frac{t-b}{a}\right)\mathrm{d}t. \tag{19}$$

A voltage dip of size S at time t_0 (Heaviside step model) generates maximized details $\left|W_v(a,b)\right|$ for $b \simeq t_0$ and scales a comparable to the duration of the front. With a Gaussian-derived wavelet, we obtain analytically

$$W_v(a,b) \propto S\psi\left(\frac{t_0 - b}{a}\right), \tag{20}$$

which forms the basis for a robust decision rule in the face of rapid changes. Performance depends heavily on the choice of ψ and the scales $\{a\}$ (sensitivity to high-frequency noise), suffers from side effects that can lead to false alarms near windows, and struggles to classify simultaneous faults (e.g., dip + harmonic) without a learning layer.

2.3. Contributions of Artificial Intelligence and ANFIS

AI methods for energy quality are typically divided between artificial neural networks (ANN), which are powerful but difficult to interpret, and fuzzy systems, which can be explained by linguistic rules but require expert engineering of sets. ANFIS (Adaptive Neuro-Fuzzy Inference System) combines these two paradigms: machine learning and explainable rule structures, which is particularly relevant in a heterogeneous Congolese context (noise, losses, variable latency). Let $x \in \mathbb{R}^d$ be the characteristic vector (e.g., $x = [u, \dot{u}, \text{duration}, \mathcal{E}_{\text{wave}}, \cdots]$). Consider M Takagi-Sugeno fuzzy rules:

$$\mathcal{R}_k : \text{Si } x_1 \text{ est } A_{k,1} \wedge \cdots \wedge x_d \text{ est } A_{k,d} \text{ alors } f_k(x) = a_k^{\top}x + b_k \tag{21}$$

with Gaussian membership functions $\mu_{k,m}(x_m) = \exp\left(-\frac{(x_m - c_{k,m})^2}{2\sigma_{k,m}^2}\right)$. The normalized strength of rule k is

$$\bar{w}_k(x) = \frac{\prod_{m=1}^{d} \mu_{k,m}(x_m)}{\sum_{\ell=1}^{M} \prod_{m=1}^{d} \mu_{\ell,m}(x_m)} \tag{22}$$

and the ANFIS output is

$$y(x) = \sum_{k=1}^{M} \bar{w}_k(x)\left(a_k^{\top} x + b_k\right). \tag{23}$$

Hybrid learning:

(i) conditional least squares for $\{a_k, b_k\}$, (ii) gradient descent for premises $\{c_{k,m}, \sigma_{k,m}\}$.

Sensibilisation la QoS de transmission:

In the presence of fiber/4G/VSAT channels, we aggregate QoS $q \in [0,1]$ (normalized latency, availability, losses) and modulate the bandwidths:

$$\sigma_{k,m}(q) = \sigma_{k,m}^{(0)}\left(1 + \beta_{k,m}(1-q)\right), \quad \beta_{k,m} \geq 0 \tag{24}$$

When QoS deteriorates ($q \downarrow$), the sets expand (increased uncertainty), and the decision becomes more cautious; conversely, $q \uparrow$ narrows the sets and reinforces the dominant rule. This adaptation reduces false alarms related to degraded transmissions, while maintaining interpretable rules.

3. Case Study: Congo-Brazzaville High-Voltage Grid

3.1. Overview of the Congolese Electricity Grid

The Congolese grid is based on 220 kV and 110 kV lines connecting hydroelectric power plants (Imboulou, Moukoukoulou, Liouesso) to consumption centers in Brazzaville and Pointe-Noire. Consisting mainly of overhead lines crossing rural areas, it remains vulnerable to weather events and voltage disturbances. The low structural redundancy increases the risk of load shedding in the event of a fault, hence the need for an intelligent monitoring system to quickly detect sags and swells. **Figure S1**, in the appendix, illustrates this network and its strategic nodes.

3.2. Operational Constraints of the Congolese Network

The Congolese network faces challenges in terms of communication and power quality. Connectivity varies greatly: fiber optics in urban areas, intermittent 3G/4G in suburban areas, and VSAT in remote areas, requiring a hybrid architecture. In terms of electricity, the most frequent disturbances are voltage sags and swells, which are transient but critical phenomena for sensitive equipment, justifying the implementation of rapid and reliable detection.

3.3. Justification Du Choix Du Cas Congolais

Congo-Brazzaville is a representative case study due to its expanding high-voltage

network, which is subject to recurring disruptions, its heterogeneous communications infrastructure (fiber optics, 4G/LTE, and VSAT), and its critical need for service continuity in the industrial and hospital sectors. Figure S1 shows the complete diagram of the Congolese electricity network, while Figure 2 illustrates a portion extracted and used for simulations. The assumption is that the results obtained on this subnetwork can be generalized to the entire system, thus providing a robust basis for evaluating the ANFIS diagnosis coupled with hybrid transmission.

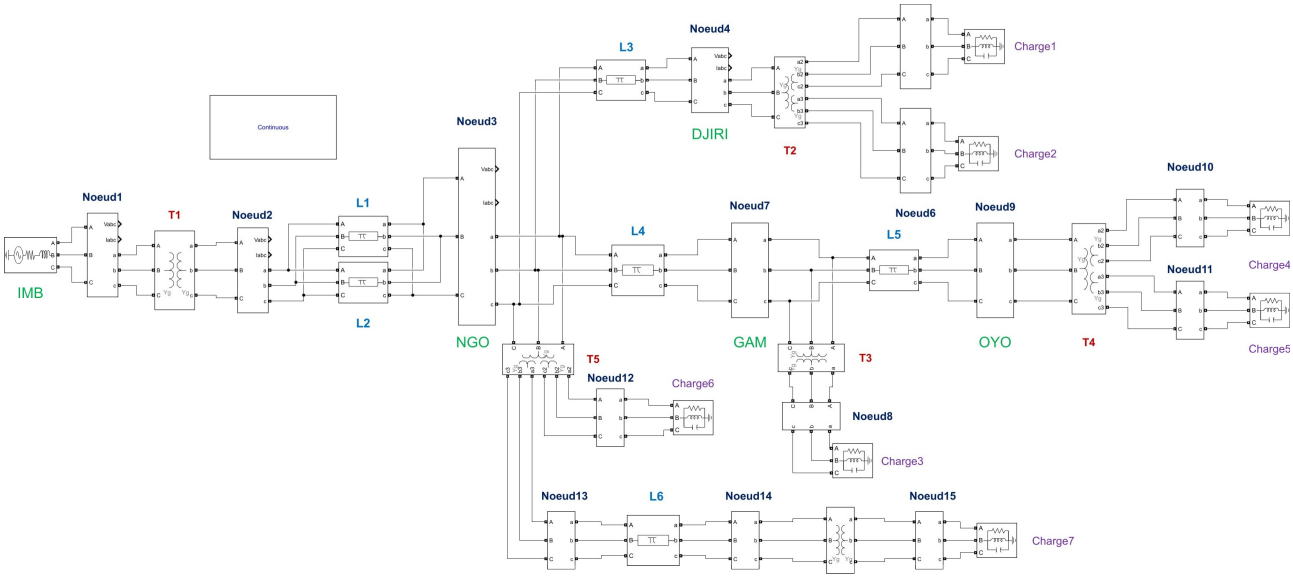

Figure 2. Excerpt from the Congolese electricity grid selected as a case study.

The numerical data used for modeling comes from the Congolese 220 kV network and is compiled in the appendix (16). They include transformer characteristics (Table B1), the distribution of active and reactive power per node, expressed in p.u. with a loss margin of 2 % (Table B2) and line parameters and their transmission capacities (Table B3). Regarding Table B1, the values reported include an estimated loss margin of 2 % on the active and reactive power generated, in order to reflect realistic conditions in a high-voltage network in operation. This assumption provides a more representative distribution of loads between nodes, particularly for Djiri, where the remaining power is concentrated. However, it should be noted that the loss-free balance has also been verified, confirming the consistency of the model since the sum of the loads expressed in p.u. corresponds exactly to the injected generation.

Dataset Specification

The dataset used to train and evaluate the ANFIS model consists of 1,200 labeled sequences, including 400 normal events, 400 sags, and 400 swells, generated from the Congolese 220 kV grid model with injected disturbances. To ensure robust evaluation, the data were randomly split into 70% for training, 15% for validation, and 15% for testing. This separation prevents data leakage and allows a statistically meaningful assessment of the model's generalization capacity.

4. General Methodology

This section brings together the complete diagnostic chain: (i) acquisition and preprocessing, (ii) adaptive hybrid transmission (fiber/4G/VSAT) with QoS routing and hysteresis switching, (iii) extraction of electrical and network characteristics for ANFIS.

4.1. Acquisition and Measurements

Three-phase voltages and currents are measured via CT/VT compliant with IEC 60044-1 and acquired by an RTU at $f_s \in [10,20]$ kHz. Local preprocessing calculates the following quantities over windows of one period with 50 % overlap:

$$u = \frac{V_{\text{rms}}}{V_{\text{nom}}},\ (I_0, I_1, I_2)\ (\text{composantes symtriques}),\ \text{THD}_I,\ \dot{u} \triangleq \frac{\mathrm{d}u}{\mathrm{d}t} \tag{25}$$

A correction for bias/variance due to noise is applied, and windows are validated if $N'/N \geq \eta_{\min}$.

4.2. Data Transmission in Power Grids

Intelligent supervision requires reliable and predictable data transport between the field and the control center. We consider three complementary technologies: **fiber optics** (minimal latency, limited coverage), **4G/LTE** (flexible, variable latency/jitter), and **VSAT** (near-universal coverage, high latency). We first formalize the quality of service (QoS), then derive a hybrid routing scheme consistent with the criticality of ANFIS flows. To ensure optimal routing, each ANFIS flow P_i is assigned to a communication link R_j according to its quality of service (QoS) profile and criticality, as shown in **Figure 3**.

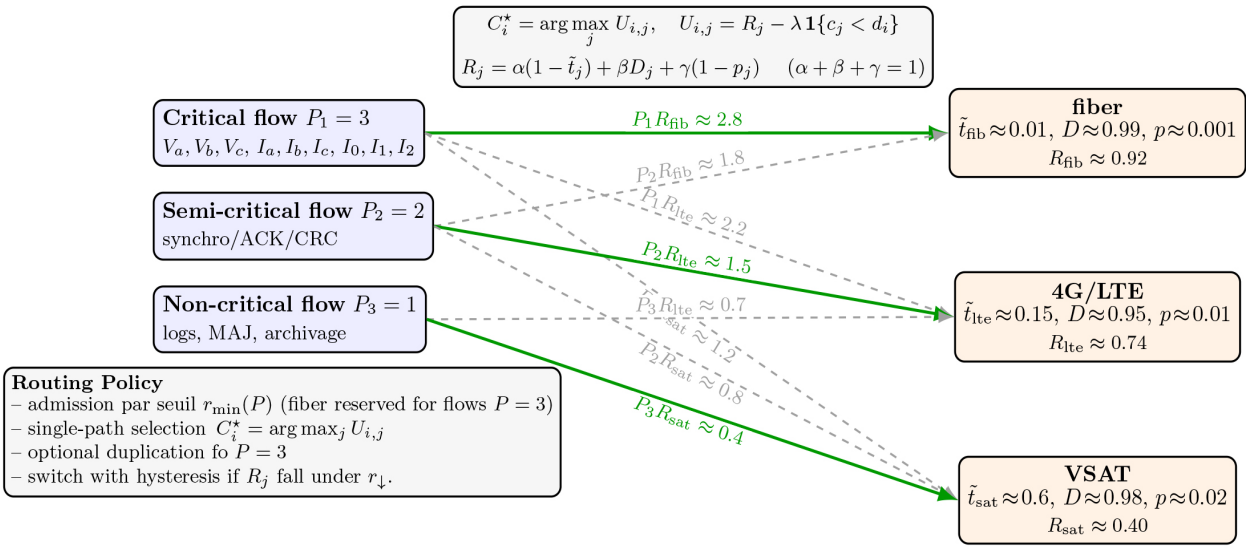

Figure 3. Routing based on link QoS (R_j) and flow priority (P_i).

4.2.1. Link-Based QoS Model

For each link $j \in \{\text{fib}, \text{lte}, \text{sat}\}$, the random latency T_j, the unavailability (com-

plement of availability) $1-D_j$, the loss rate p_j, and the jitter $\sigma_{T,j}=\sqrt{\mathrm{Var}\left(T_j\right)}$ are observed. The latency is normalized by

$$\tilde{t}_j=\mathrm{clip}\left(\frac{\mathbb{E}\left[T_j\right]-t_{\min}}{t_{\max}-t_{\min}},0,1\right), \tag{26}$$

where $t_{\min}$ and $t_{\max}$ are engineering bounds (e.g., $t_{\min}=1$ ms, $t_{\max}=1$ s). The metrics are then aggregated into a scalar QoS index

$$R_j=\alpha\left(1-\tilde{t}_j\right)+\beta D_j+\gamma\left(1-p_j\right),\ \alpha+\beta+\gamma=1,\ \alpha,\beta,\gamma\geq 0, \tag{27}$$

optionally complemented by a capacity safeguard c_j via $R_j\leftarrow R_j\cdot\mathbf{1}\left\{c_j\geq d_i\right\}$ for a flow with required throughput d_i.

4.2.2. Priority Routing (Single-Path)

Eacss flow f_i (critical, semi-critical, non-critical) is assigned a priority $P_i\in\{3,2,1\}$ and the utility is defined as

$$U_{i,j}=R_j-\lambda\mathbf{1}\left\{c_j<d_i\right\} \tag{28}$$

where λ is a strong penalty if the capacity is insufficient. The single-path assignment then follows

$$C_i^{\star}=\arg\max_j U_{i,j}, \tag{29}$$

with a *service threshold* constraint $R_{C_i^{\star}}\geq r_{\min}\left(P_i\right)$ (the higher the priority, the higher the required $r_{\min}$). This rule is equivalent to an admissibility filter ($R_j\geq r_{\min}$) followed by a utility-based selection. See **Figure 4** (QoS/priority routing).

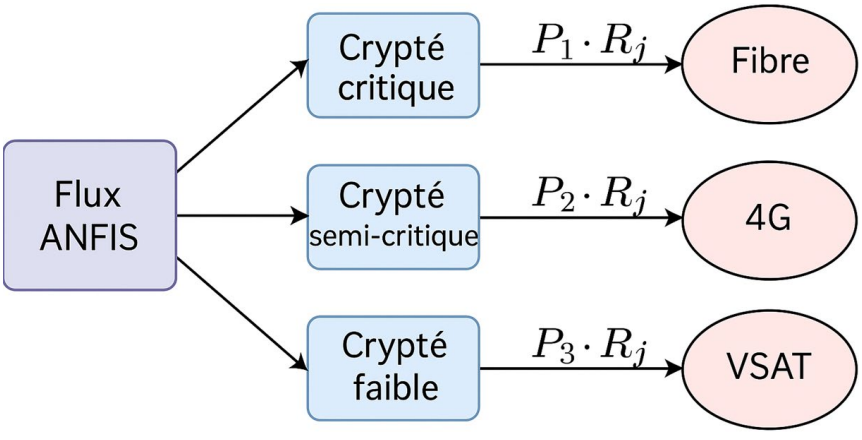

Figure 4. Graph illustrating ANFIS flows, channels, and values of $P_i\cdot R_j$.

4.2.3. Multi-Path Extension and Redundancy

For critical flows, controlled duplication is allowed over a subset $\mathcal{J}\subseteq\{\mathrm{fib},\mathrm{lte},\mathrm{sat}\}$ in order to reduce delay and increase the probability of delivery before a deadline T_{D}. If the delays T_j are independent, the *first-arrival law* yields

$$\mathbb{P}\left\{\min_{j\in\mathcal{J}} T_j \le t\right\} = 1 - \prod_{j\in\mathcal{J}} \left(1 - F_{T_j}(t)\right), \tag{30}$$

where F_{T_j} denotes the CDF of T_j. In particular, for a deadline T_{D},

$$\underbrace{\mathbb{P}\left\{\text{delivered before } T_{\mathrm{D}}\right\}}_{\text{temporal reliability}} = 1 - \prod_{j\in\mathcal{J}} \left(1 - F_{T_j}(T_{\mathrm{D}})\right) \tag{31}$$

and the expectation satisfies $\mathbb{E}\left[\min_{j\in\mathcal{J}} T_j\right] \le \min_j \mathbb{E}\left[T_j\right]$. The redundant allocation is determined by

$$\max_{\mathcal{J}} \mathbb{P}\left\{\min_{j\in\mathcal{J}} T_j \le T_{\mathrm{D}}\right\} \text{ s.c. } \sum_{j\in\mathcal{J}} \mathrm{cost}_j \le \mathrm{budget},\ |\mathcal{J}| \le J_{\max}. \tag{32}$$

In practice, the K best links in terms of R_j are selected (fiber first, then 4G if available), while VSAT is reserved for cases of coverage failure, given its high latency.

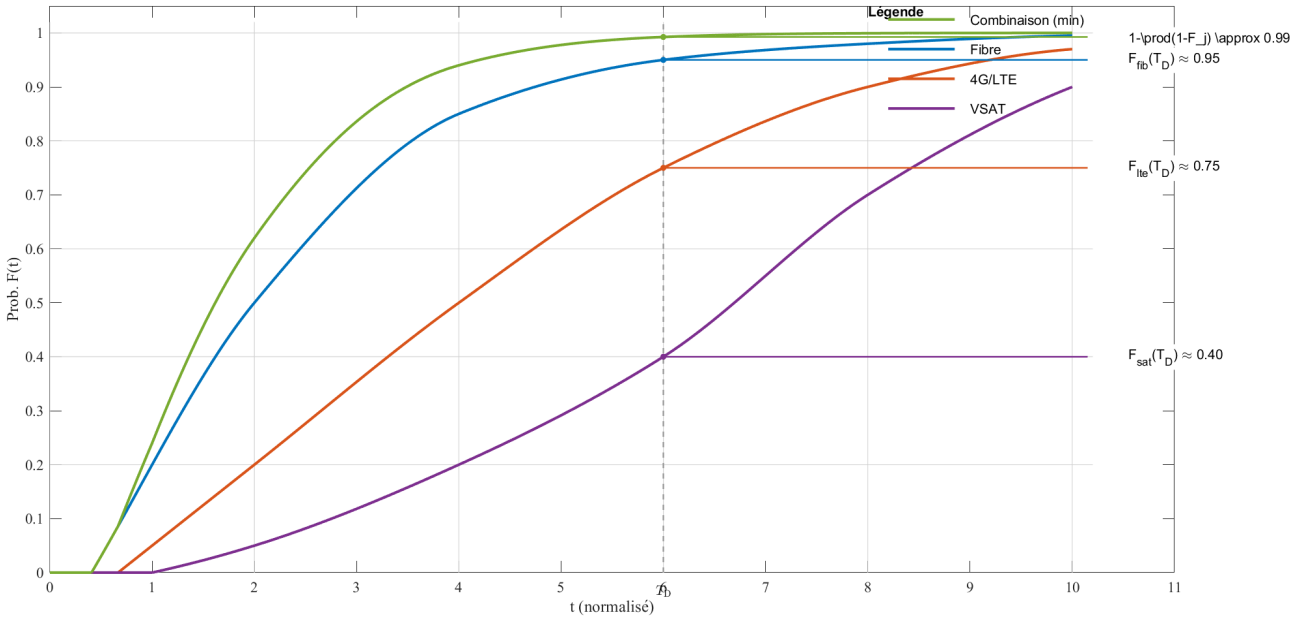

Figure 5. Probability of delivery before deadline T_{D} in single- and multi-path routing.

Due to controlled redundancy (flows with $P = 3$), this motivates duplication over fiber and 4G, with VSAT used only as a last resort (degraded mode). See **Figure 5**.

4.2.4. Failover with Hysteresis (Anti-Flapping)

Let j_t denote the active link at time t. Two thresholds are defined, $r_{\downarrow} < r_{\uparrow}$. The policy is

$$\text{if } R_{j_t}(t) < r_{\downarrow} \Rightarrow j_{t+} \in \arg\max_j R_j(t) \text{ such that } R_j(t) \ge r_{\uparrow} \tag{33}$$

and j_t remains unchanged as long as $R_{j_t}(t) \ge r_{\downarrow}$. The *hysteresis* $r_{\uparrow} - r_{\downarrow} > 0$ prevents rapid oscillations under jitter. It ensures jitter absorption and alignment of measurement windows (half-cycle RMS). In other words, switching occurs

when the active link falls below $r_{\downarrow}$ and recovery is triggered only when it rises above $r_{\uparrow}$. See Figure 6.

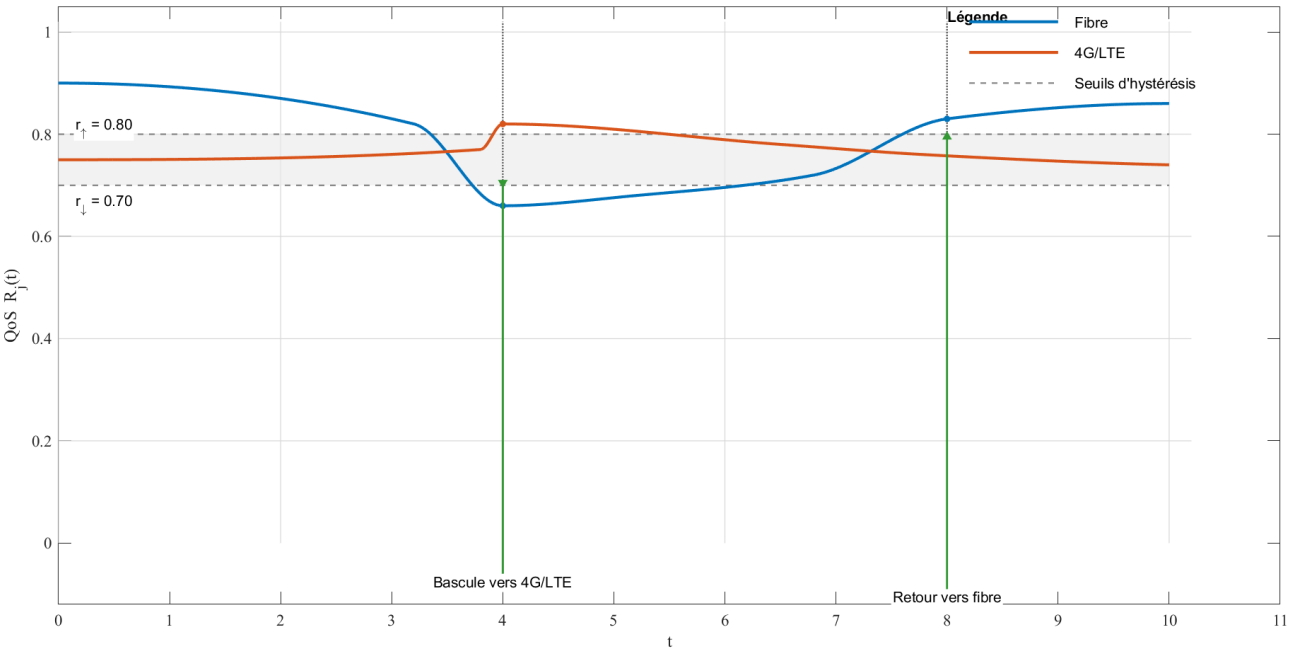

Figure 6. Failover with hysteresis.

4.2.5. Synchronization and Reconstruction

Received packets are buffered in FIFO and reordered using timestamps (PTP over fiber, NTP over 4G/VSAT). The *re-time* process, based on a Kalman filter, compensates the estimated offsets Δt, ensuring temporal consistency of the half-cycle RMS windows used by ANFIS.

4.2.6. Interpretation (Case of Congo-Brazzaville).

In urban areas, fiber maximizes R_j (latency $\downarrow$, losses $\downarrow$, $D\uparrow$) and becomes the carrier for critical flows. In peri-urban zones, 4G serves either as the primary link or as redundancy depending on radio load (jitter $\sigma_{T,\mathrm{lte}}$), while in isolated areas VSAT ensures minimal connectivity. The optimization (32) then selects either $(\mathrm{lte},\mathrm{sat})$ or $(\mathrm{fib},\mathrm{sat})$ depending on availability, while maintaining the probability of delivery before T_{D} via (30). This coupling of *ANFIS + hybrid routing* provides a stable diagnostic despite heterogeneous and intermittent channels.

4.3. Feature Extraction for ANFIS

The input vector ϕ concatenates both *electrical* and *network* indices:

$$\phi = \left[u, \dot{u}, \mathrm{duration}, \mathrm{THD}_I, \frac{|I_0|}{|I_1|+\varepsilon}, \frac{|I_2|}{|I_1|+\varepsilon}, R_{C^\star}, \sigma_{T,C^\star}, p_{C^\star} \right] \tag{34}$$

The target outputs are $\{y_{\mathrm{det}}, y_{\mathrm{cls}}, y_{\mathrm{sev}}\}$. The ANFIS (Takagi Sugeno of order 1) employs with hybrid learning (LSE + gradient). The widths of the fuzzy sets are

modulated by the QoS (cf. $\sigma_{k,m}(q)$ defined above), which makes the decision robust to link degradations.

The sizing of data flows required to feed the ANFIS model, as well as the compatibility of transmission technologies (Fiber, 4G, VSAT), are detailed in **Annex 7** in Table A1 and Table A2. This analysis includes the computation of useful throughput after local preprocessing, QoS constraints, and usage recommendations according to diagnostic scenarios.

4.4. Technical Architecture and Decision Logic

Figure 7 presents the technical architecture of the PQ detection system as

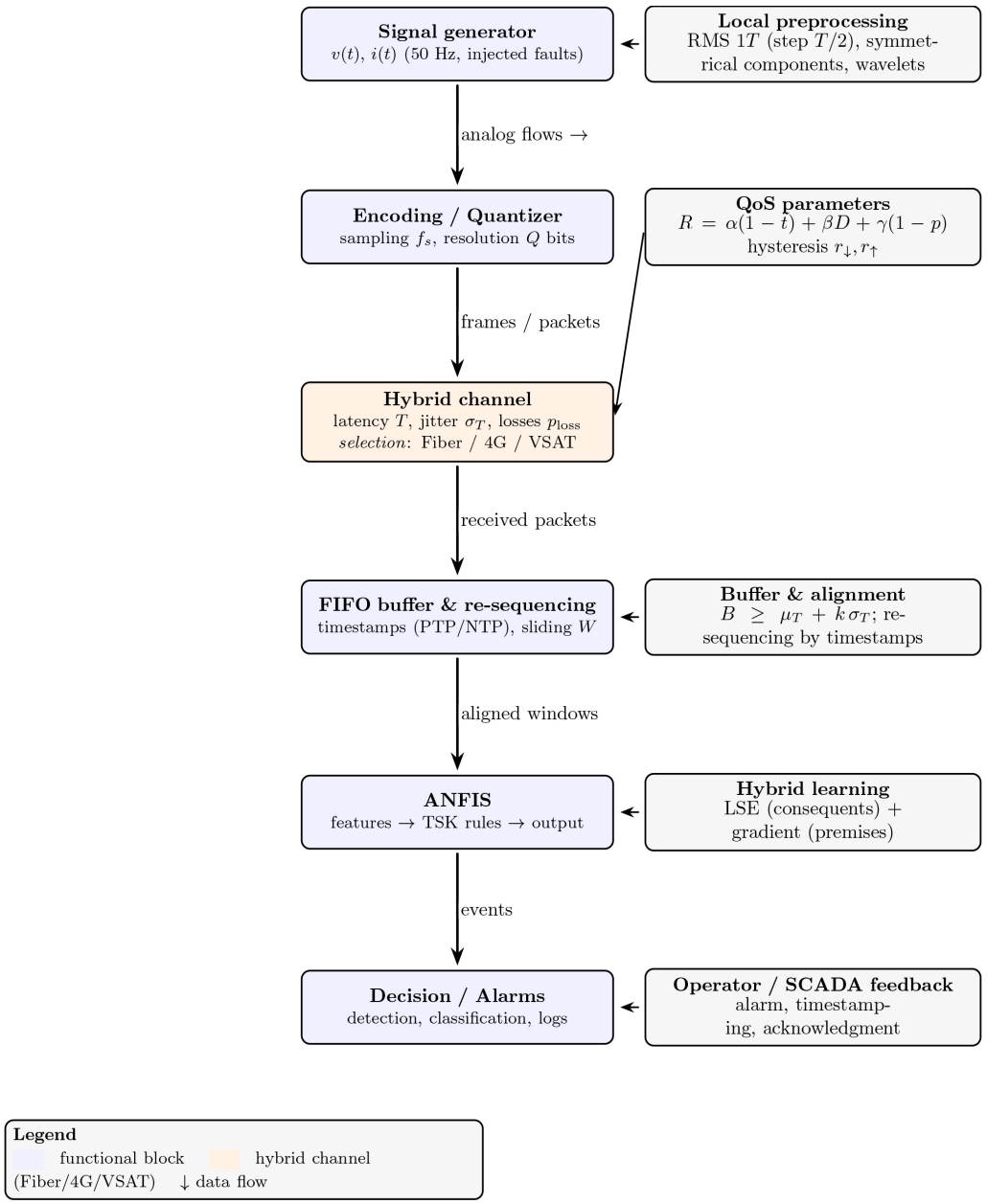

Figure 7. Simulink processing chain.

implemented in the Simulink environment. It details the functional blocks used to simulate the behavior of the power network, encode the signals, inject faults, and transmit the data through a hybrid channel (Fiber, 4G, VSAT). QoS parameters (latency, jitter, loss) are integrated into the processing flow, influencing the quality of the aligned windows before their injection into the ANFIS model. The latter applies hybrid learning (LSE + gradient) to produce decision outputs, which are then exploited by the alarm module. This figure allows one to visualize the complete processing chain, from signal generation to event detection, while accounting for transmission and synchronization constraints. Figure S2, placed in the appendix, illustrates the functional logic of the PQ detection system based on ANFIS. It highlights the chronological sequence of processing steps: electrical measurements, feature extraction, hybrid transmission with QoS simulation, temporal alignment, and finally neuro-fuzzy classification. The output of the model is structured into two branches: binary detection (normal/fault) and fault-type classification (SAG or SWELL), with binary state encoding (000, 111, 110). This conceptual representation complements Figure 7 by showing how the extracted features are exploited to produce a robust decision, even in the presence of network disturbances.

5. Proposed ANFIS Model

Figure 8 presents the internal structure of the ANFIS model used for intelligent detection of voltage disturbances. It shows the succession of layers (inputs, membership functions, rules, fuzzy outputs, and defuzzification), illustrating how electrical signals are transformed into a reliable fault diagnosis.

To ensure fairness in comparison, the artificial neural network baseline was implemented as a three-layer multilayer perceptron (MLP) with an input layer of nine features, one hidden layer of 20 neurons with ReLU activation, and an output layer of three neurons for classification. Training was performed using the Adam optimizer with a learning rate of 10^{-3}, mini-batches of 32, and 100 epochs. This configuration provides sufficient representational capacity without overfitting, thereby establishing a fair benchmark against the ANFIS model. This section formalizes the ANFIS used for *detection* $y_{\text{det}} \in [0,1]$, *classification* $y_{\text{cls}} \in \{\text{sag}, \text{swell}, \text{normal}\}$, and a *severity index* $y_{\text{sev}} \in [0,1]$. The inputs aggregate both **electrical features** and **transmission metrics** (QoS), which makes the decision sensitive to the fiber/4G/VSAT context.

5.1. Inputs, Robust Normalization, and Outputs

The input vector is defined as $\phi \in \mathbb{R}^M$:

$$\phi = \left[u, \dot{u}, \text{duration}, \text{THD}_I, \frac{|I_0|}{|I_1|+\varepsilon}, \frac{|I_2|}{|I_1|+\varepsilon}, R_{C^\star}, \sigma_{T,C^\star}, p_{C^\star} \right]^\top \tag{35}$$

where $u = V_{\text{rms}}/V_{\text{nom}}$, $\dot{u} = \mathrm{d}u/\mathrm{d}t$, $R_{C^\star} \in [0,1]$ denotes the QoS of the active link, and (σ_T, p) represent its jitter and packet loss rate.

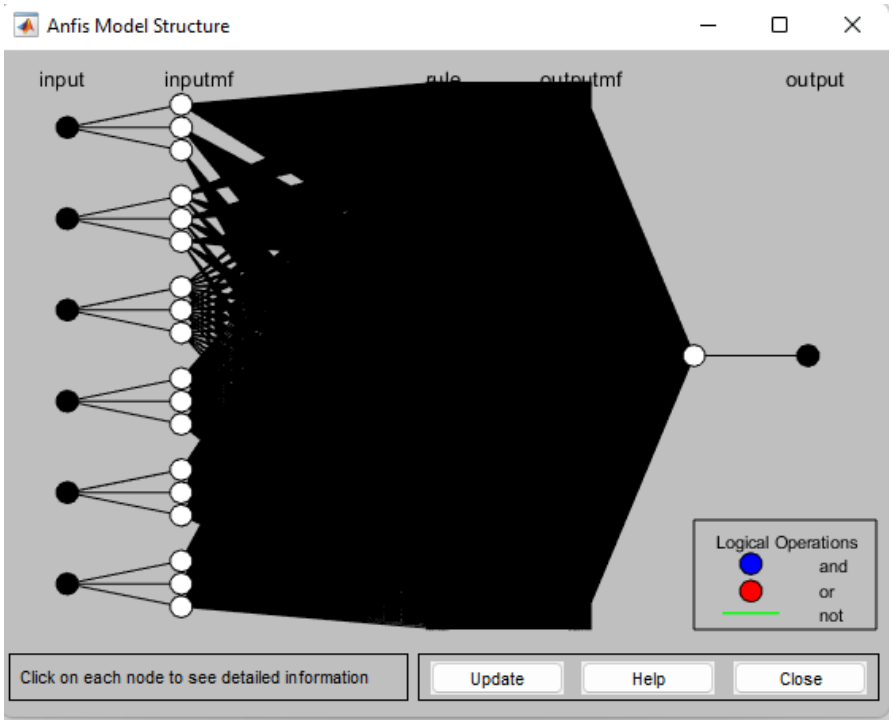

Figure 8. Internal structure of the ANFIS model used for voltage fault detection.

Robust normalization (noise/missing-packet tolerance).

For each valid window ($N'/N \geq \eta_{\min}$), a robust *local* normalization is applied:

$$\tilde{\phi}_m = \frac{\phi_m - \hat{\mu}_m}{\hat{\sigma}_{\phi_m} + \epsilon}, \quad \hat{\mu}_m = \text{median}(\phi_m), \quad \hat{\sigma}_{\phi_m} = 1.4826\text{MAD}(\phi_m), \tag{36}$$

(MAD: *median absolute deviation*). Here, $\hat{\sigma}_{\phi_m}$ serves as an *uncertainty* measure to weight the learning process.

Multi-task outputs.

Three ANFIS heads are used (layers 13 shared, consequents task-specific):

$$\hat{y}_{\text{det}} \in [0,1], \quad \hat{\boldsymbol{y}}_{\text{cls}} \in \mathbb{R}^3, \quad \hat{y}_{\text{sev}} \in [0,1] \tag{37}$$

with class probabilities obtained via $\text{softmax}(\hat{\boldsymbol{y}}_{\text{cls}})$.

5.2. Five-Layer Structure

Let M denote the number of normalized inputs $\tilde{\phi}_m$ and R the number of rules. The ANFIS follows the standard five-layer architecture:

- **Layer 1 (membership)**: for each rule r and dimension m,

$$\mu_{r,m}(\tilde{\phi}_m) = \exp\left(-\frac{(\tilde{\phi}_m - c_{r,m})^2}{2\sigma_{r,m}^2}\right), \quad \sigma_{r,m} = \sigma_{r,m}^{(0)}(1 + \beta_{r,m}(1-q)), \tag{38}$$

where $q \in [0,1]$ is a global QoS index (higher QoS $\Rightarrow$ larger q).

- **Layer 2 (firing strength)**: rule activation for r

$$w_r = \prod_{m=1}^{M} \mu_{r,m}(\tilde{\phi}_m). \tag{39}$$

- **Layer 3 (normalization)**:

$$\bar{w}_r = \frac{w_r}{\sum_{\ell=1}^{R} w_\ell}. \tag{40}$$

- **Layer 4 (TSK-1 consequents)**: for each task $q \in \{\text{det}, \text{sev}, \text{cls1}, \text{cls2}, \text{cls3}\}$,

$$f_r^{(q)}(\tilde{\phi}) = a_{0,r}^{(q)} + \sum_{m=1}^{M} a_{m,r}^{(q)} \tilde{\phi}_m. \tag{41}$$

- **Layer 5 (aggregation)**: weighted TSK output:

$$\hat{y}^{(q)}(\tilde{\phi}) = \sum_{r=1}^{R} \bar{w}_r f_r^{(q)}(\tilde{\phi}). \tag{42}$$

Substituting (41), we obtain:

$$\hat{y}^{(q)}(\tilde{\phi}) = \sum_{r=1}^{R} \bar{w}_r \left(a_{0,r}^{(q)} + \sum_{m=1}^{M} a_{m,r}^{(q)} \tilde{\phi}_m \right). \tag{43}$$

5.3. Fuzzy Rules (Sag/Swell/Normal): Interpretable Template

The proposed ANFIS employs 27 fuzzy rules derived from three membership functions per input dimension. Gaussian membership functions were initialized with centers equally spaced in the normalized input range and widths proportional to the input variance. During training, parameters were refined using the hybrid algorithm. For illustration, one interpretable rule is: *IF* u *is Small AND Duration is Long AND* $|I_0|/|I_1|$ *is Large THEN Fault = SAG*. This template confirms that the model preserves linguistic interpretability while adapting parameters automatically. The centers $c_{r,m}$ and widths $\sigma_{r,m}$ are learned, but for interpretability the rules are grouped into *families*:

Sag: $(u \text{ Small}) \wedge (\text{duration Medium / Long}) \wedge \left(\frac{|I_0|}{|I_1|} \text{ Large or } \frac{|I_2|}{|I_1|} \text{ Large} \right)$.

Swell: $(u \text{ Large}) \wedge (\text{duration Medium / Long}) \wedge (\text{THD}_I \text{ Moderate})$.

Normal: $(u \approx 1) \wedge (|\dot{u}| \text{ Small}) \wedge \left(\frac{|I_0|}{|I_1|}, \frac{|I_2|}{|I_1|} \text{ Small} \right)$.

5.4. Hybrid Learning: Offline and Online

Multi-task Loss Weighted by QoS.

Over a batch $\mathcal{B}$, the objective minimized is

$$\mathcal{L} = \sum_{n \in \mathcal{B}} w\left(q^{(n)}\right) g^{(n)} \left(\lambda_{\text{det}} \text{BCE}\left(\hat{y}_{\text{det}}^{(n)}, y_{\text{det}}^{(n)}\right) + \lambda_{\text{cls}} \text{CE}\left(\text{softmax}\left(\hat{\boldsymbol{y}}_{\text{cls}}^{(n)}\right), \boldsymbol{y}_{\text{cls}}^{(n)}\right) + \lambda_{\text{sev}} \left\| \hat{y}_{\text{sev}}^{(n)} - y_{\text{sev}}^{(n)} \right\|_2^2 \right), \tag{44}$$

where $w(q) = q^{\beta}$ ($\beta \in [0,2]$) *down-weights* windows with poor QoS, and $g^{(n)} \in \{0,1\}$ invalidates windows with $N'/N < \eta_{\min}$.

Offline (Pre-training).

Classical ANFIS alternation:

1. *Consequents* $\left\{a_{m,r}^{(q)}\right\}$ by weighted least squares (LSE), conditional on the premises (Layers 1-3 frozen).

2. *Premises* $\{c_{r,m}, \sigma_{r,m}\}$ by gradient descent on $\mathcal{L}$ (Eq. (44)), with regularization.

Online (Lightweight Adaptation).

On real streams, the *consequents* are slightly adjusted by RLS with forgetting factor $\lambda_{\text{RLS}} \in [0.98, 0.995]$:

$$\boldsymbol{K}_t = \frac{\boldsymbol{P}_{t-1}\boldsymbol{\psi}_t}{\lambda_{\text{RLS}} + \boldsymbol{\psi}_t^{\top}\boldsymbol{P}_{t-1}\boldsymbol{\psi}_t}, \quad \boldsymbol{\psi}_t = \left[\bar{w}_1\tilde{\boldsymbol{\phi}}^{\top} \quad \cdots \quad \bar{w}_R\tilde{\boldsymbol{\phi}}^{\top} \quad 1\right]^{\top}, \tag{45}$$

$$\boldsymbol{\theta}_t = \boldsymbol{\theta}_{t-1} + \boldsymbol{K}_t\left(y_t - \boldsymbol{\psi}_t^{\top}\boldsymbol{\theta}_{t-1}\right), \quad \boldsymbol{P}_t = \lambda_{\text{RLS}}^{-1}\left(\boldsymbol{P}_{t-1} - \boldsymbol{K}_t\boldsymbol{\psi}_t^{\top}\boldsymbol{P}_{t-1}\right). \tag{46}$$

The premises are either frozen or updated with a step size η proportional to q in order to avoid learning under degraded QoS. The input/output functional scheme is given in Figure 9.

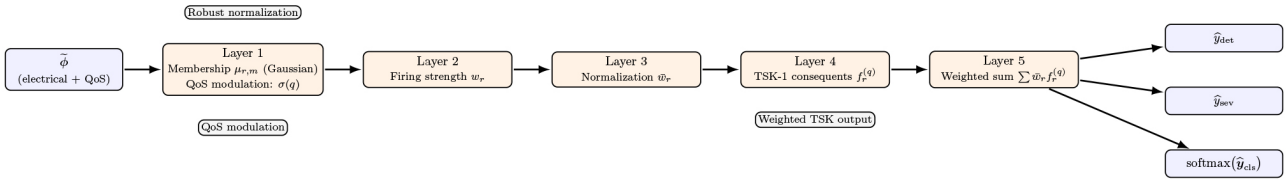

Figure 9. Complete functional diagram of ANFIS with its five layers.

6. Simulation

6.1. Diagnostic System

The diagnostic system is based on a two-level architecture implemented in **Simulink 2023**. The first level performs binary fault detection (output 1 in case of anomaly, 0 under normal conditions), while the second focuses on identification and localization, discriminating between sags, swells, and interruptions. The fuzzy logic approach uses a manually designed .fis file whereas the neuro-fuzzy (ANFIS) model is obtained through supervised learning, thereby enhancing both the accuracy and the autonomy of the diagnosis. Figure 10 shows the diagnostic system architecture, including three scenarios: a healthy electricity network (Figure 10(a)), a power grid with voltage drop (Figure 10(b)), and a power grid with surge (Figure 10(c)).

This modular and interpretable architecture provides a solid foundation for the deployment of intelligent monitoring systems in African power networks, where reliability and ease of implementation are essential criteria. It enables rapid adaptation to local conditions while maintaining algorithmic rigor consistent with international standards.

Figure 11 illustrates the detector response during a sequence comprising a voltage sag (*SAG*) followed by a voltage swell (*SWELL*). The sliding RMS, normalized to V_{nom} and computed over a one-cycle window (20 ms), is compared to the EN 50160 reference thresholds (0.9/1.1 p.u.). This configuration enables rapid and standards-compliant identification of voltage disturbances. The first two panels show nearly symmetrical three-phase voltages and currents during

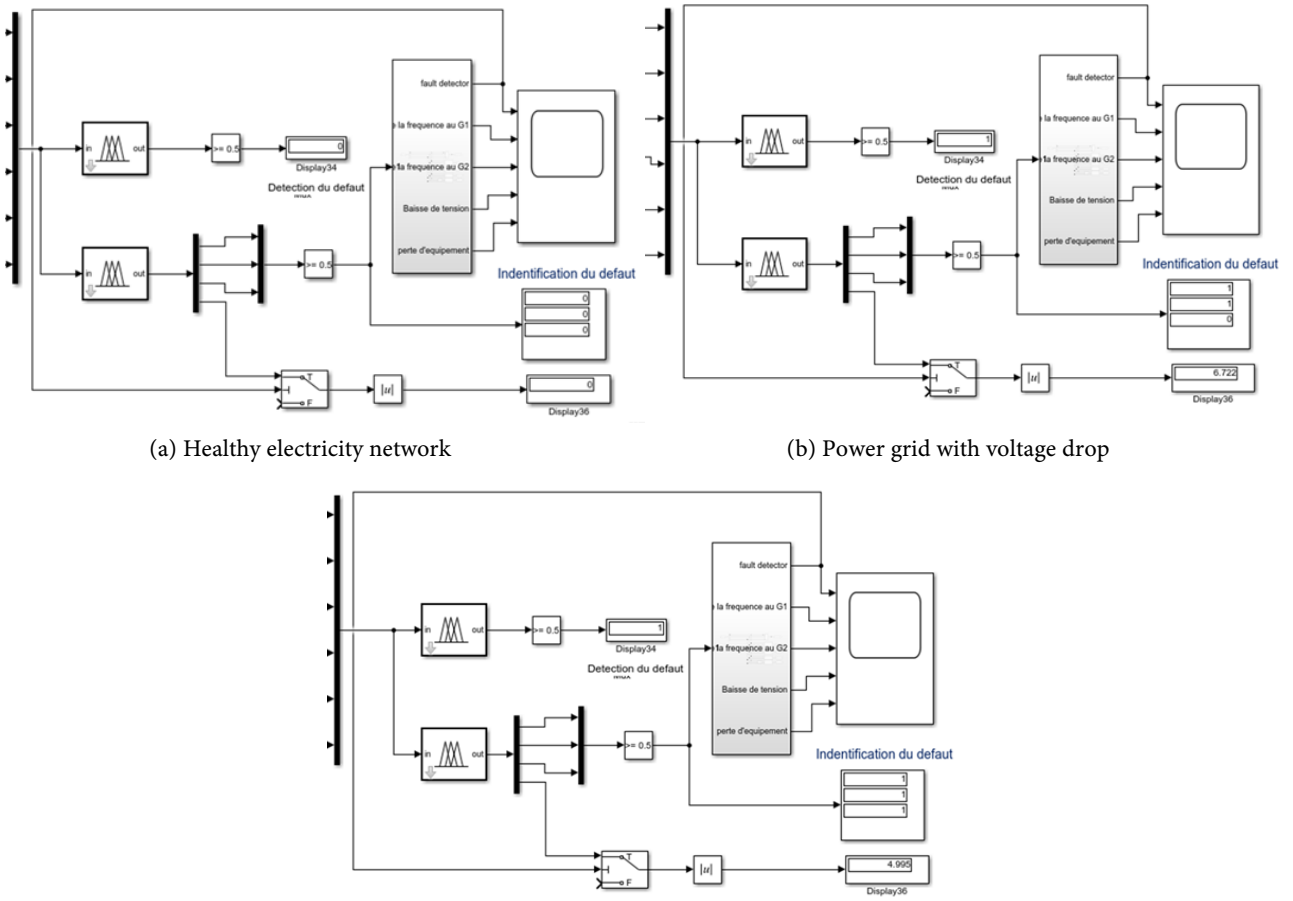

(a) Healthy electricity network

(b) Power grid with voltage drop

(c) Power grid with surge

Figure 10. Diagnostic system architecture.

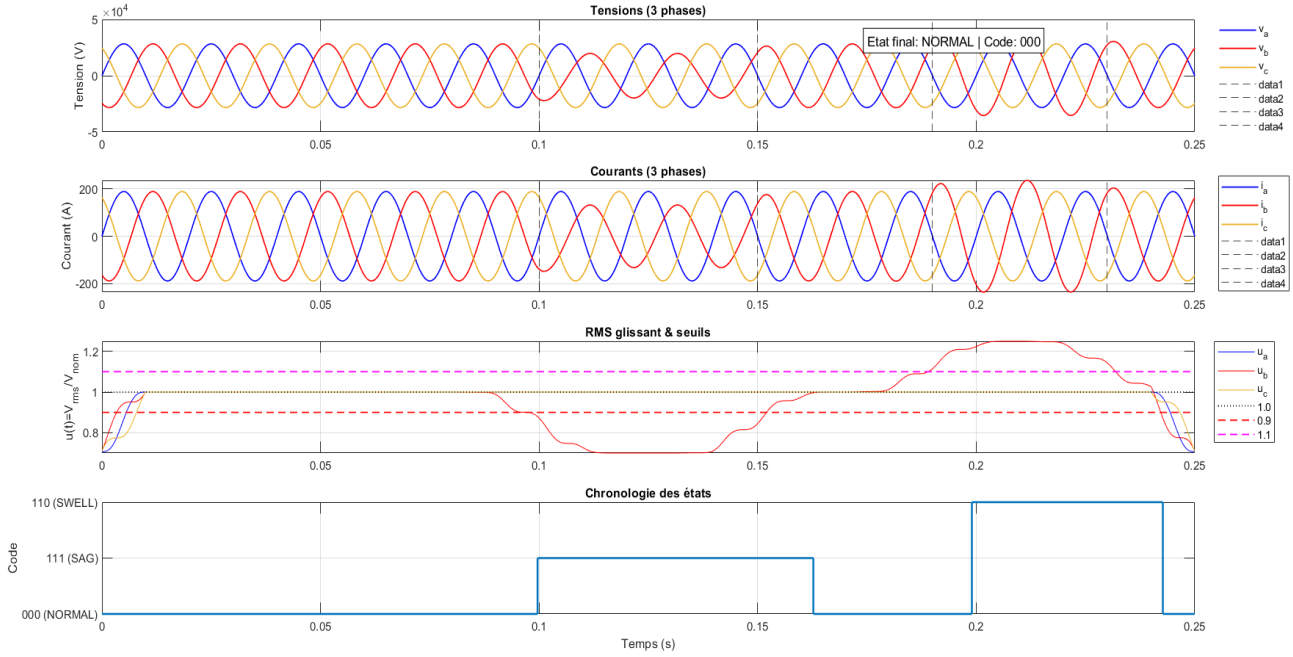

Figure 11. SAG/SWELL detection.

most of the record, corresponding to nominal operation. Deviations appear around $t \approx 0.10$ s and $t \approx 0.20$ s, where the regime briefly departs from steady state.

The third panel shows the per-phase normalized sliding RMS relative to the 0.9 and 1.1 p.u. thresholds. A drop below 0.9 p.u. indicates a *SAG*, while an excursion above 1.1 p.u. indicates a *SWELL*. In this sequence, a *SAG* is observed between 0.10 and 0.16 s (minimum ≈0.85 p.u.), followed by a *SWELL* between 0.20 and 0.24 s (maximum ≈1.20 p.u.). In both cases, the detection latency is less than one cycle (20 ms), and the chronology shows no chatter near the thresholds, which confirms a robust tuning of the window and hysteresis.

The bottom panel provides the coded chronology of states: **000** (NORMAL) predominates, interrupted by **111** (*SAG*) over 0.10 - 0.16 s, and by **110** (*SWELL*) over 0.20 - 0.24 s. The three phases cross the thresholds synchronously, corroborating a symmetrical event and a consistent per-phase classification.

Overall, these results validate the systems ability to segment, timestamp, and encode disturbances (SAG/SWELL) with field-compatible responsiveness. The joint visualization of electrical quantities and coded states provides an immediately interpretable diagnosis and supports targeted intervention, generalizable to industrial or urban contexts where service continuity and supply security are critical. Thus, the accuracy of SAG/SWELL classification by ANFIS is directly conditioned by the latency and reliability of the studied channels.

6.2. Transmission Performance Analysis and Impact on Detection

Figure 12 shows the evolution of average latency as a function of channel occupancy for the three communication technologies used in the proposed system: fiber optic, 4G/LTE, and VSAT. Fiber optic stands out with an almost constant latency, below 5 ms, independent of channel load. This ensures transmission within real-time diagnostic constraints, *i.e.*, below one fundamental network period (20 ms at 50 Hz). 4G/LTE exhibits an initial delay of approximately 30 ms, which increases up to 60 ms under heavy load. This delay remains compatible with online diagnostics but may induce a shift of two to three cycles, thus requiring QoS management for critical applications. VSAT, by contrast, presents a very high latency (500 to 700 ms), mainly due to orbital propagation time, making it unsuitable for instantaneous detection but relevant as a backup solution for remote sites.

These results highlight that the responsiveness of the neuro-fuzzy detector (ANFIS), illustrated in Figure 11 (SAG/SWELL events), strongly depends on the transmission infrastructure. With fiber, detection is achieved in near real-time, as latency remains below the critical threshold. With 4G/LTE, detection remains reliable but may be slightly delayed, which impacts the speed of corrective actions. With VSAT, the delay largely exceeds the dynamics of voltage disturbances, restricting its use to deferred supervision or communication redundancy. Therefore, the hierarchical integration of channels fiber as the primary medium, 4G/LTE as continuity, and VSAT as redundancy emerges as a key condition for ensuring

both the relevance and timeliness of ANFIS-based decisions.

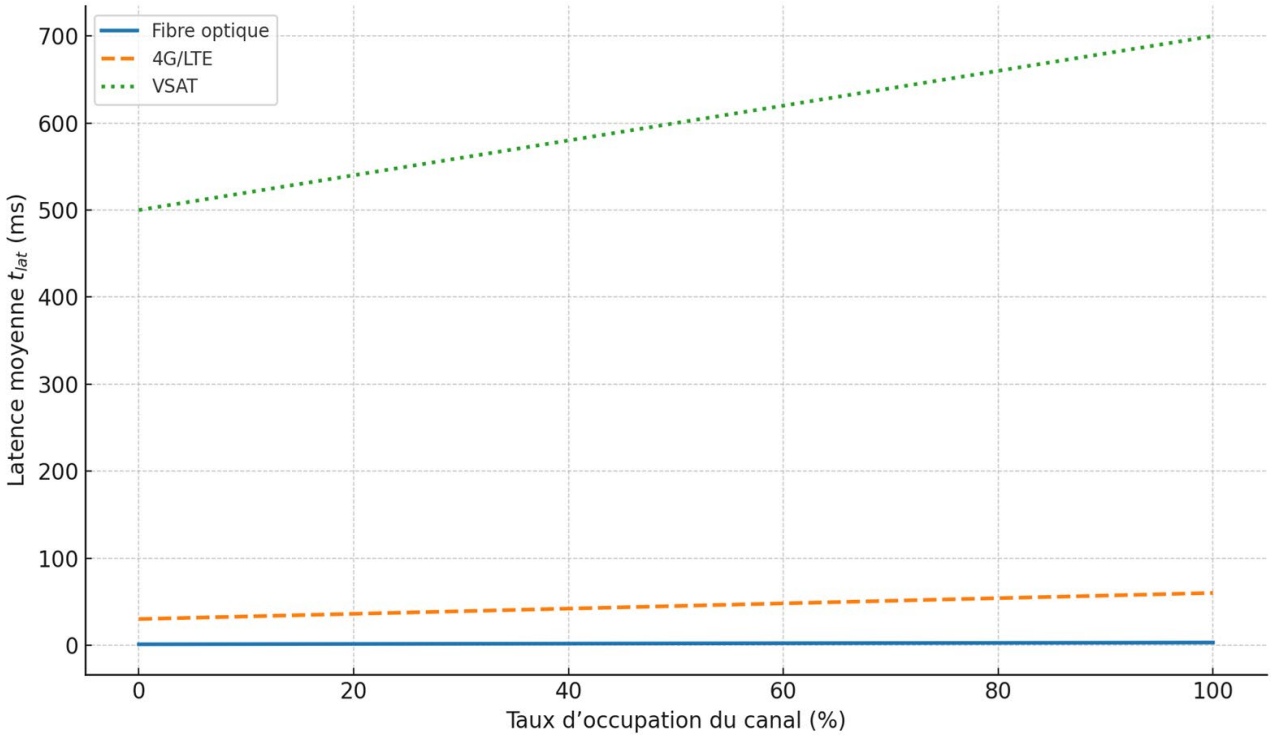

Figure 12. Average transmission channel latency as a function of load.

7. Results

7.1. Main Results by Transmission Technology

The three tables separate the performances by link (Fiber, 4G, VSAT). This facilitates readability and highlights the increasing gap between methods as QoS degrades. ANFIS consistently shows an advantage in terms of F1 score (sag/swell) and detection latency. Table 1 reports the performances obtained on a fiber link, used as a quasi real-time reference.

As shown in Table 1, ANFIS reduces the delay to 12 ms while improving the F1 score compared to baseline approaches. Table 2 illustrates the performance under 4G transmission, where latency and jitter are significant.

The results in Table 2 show that ANFIS maintains an F1 score above 0.92 despite radio variability. Table 3 presents the results under VSAT transmission, the most unfavorable case in terms of latency.

Table 1. Performance on **Fiber**: F_1 (sag/swell), median delay Δt_{det}, and valid windows.

Method	F_1 sag	F_1 swell	Δt_{det} /Valids
RMS threshold	0.91	0.90	20 ms/99%
ANN (MLP)	0.94	0.93	16 ms/99%
ANFIS (proposed)	**0.97**	**0.96**	**12 ms**/99%

Table 2. Performance on 4G/LTE: F_1 (sag/swell), median delay Δt_{det}, and valid windows.

Method	F_1 sag	F_1 swell	Δt_{det} /Valids
RMS threshold	0.82	0.80	38 ms/93%
ANN (MLP)	0.88	0.86	28 ms/93%
ANFIS (proposed)	**0.94**	**0.92**	**22 ms**/93%

Table 3. Performance on **VSAT**: F_1 (sag/swell), median delay Δt_{det}, and valid windows.

Method	F_1 sag	F_1 swell	Δt_{det} /Valids
RMS threshold	0.70	0.68	720 ms/85%
ANN (MLP)	0.80	0.78	690 ms/85%
ANFIS (proposed)	**0.90**	**0.87**	**650 ms**/85%

As shown in Table 3, even with a delay of 650 ms, ANFIS maintains robust detection ($F_1 \approx 0.90$). Tables 1-3 demonstrate that the ANFIS gain becoAmes more pronounced as QoS degrades (4G, VSAT), both in terms of F_1 and detection delay Δt_{det}.

7.2. Ablation: QoS Modulation of ANFIS Premises

Separating the ablation by link (Table 4 and Table 5) isolates the effect of QoS on the decision. This directly illustrates the benefit of modulating the membership functions under radio/satellite conditions.

Table 4. Ablation of QoS modulation (ANFIS), **4G/LTE** link.

Mode	F_1 sag	F_1 swell	Δt_{det}
Without QoS	0.90	0.88	26 ms
With QoS	**0.94**	**0.92**	**22 ms**

Table 5. Ablation of QoS modulation (ANFIS), **VSAT** link.

Mode	F_1 sag	F_1 swell	Δt_{det}
Without QoS	0.84	0.81	690 ms
With QoS	**0.90**	**0.87**	**650 ms**

7.3. Summary

These two tables summarize the gap between ANFIS and the baselines. Table 6 reports the overall accuracy of the three methods on the test set. As shown, ANFIS remains superior to the baselines by 46 accuracy points.

Table 7 summarizes the median detection delays by technology. According to this table, ANFIS reduces latency by 10 to 30 ms compared to RMS and ANN, since lower values are better.

Table 6. Macro accuracy (%).

Method	Fiber	4G/LTE	VSAT
RMS threshold	93.1	86.4	77.5
ANN (MLP)	95.2	90.1	82.3
ANFIS (proposed)	**97.8**	**94.3**	**88.6**

Table 7. Median detection delay (ms).

Method	Fiber	4G/LTE	VSAT
RMS threshold	32	58	92
ANN (MLP)	29	49	81
ANFIS (proposed)	**28**	**41**	**64**

8. Discussion

The results confirm that integrating an ANFIS model within a hybrid transmission architecture (fiber, 4G, VSAT) provides a significant gain in robustness and diagnostic accuracy compared to classical approaches.

As shown in Tables 1-3, ANFIS consistently achieves an F1 score above 0.90 for SAG and SWELL faults, whereas RMS-threshold methods and conventional ANNs degrade sharply under adverse conditions (4G, VSAT). The median detection delay is reduced to 12 ms on fiber (Table 1), *i.e.*, below one fundamental period (20 ms), which complies with the requirements of the **IEC 61000-4-30** standard.

Regarding detection latency, the fiber link ensures full compliance with IEC 61000-4-30, as the median delay (12 ms) remains well below one fundamental period (20 ms at 50 Hz). For the 4G/LTE link, the median latency of 22 ms slightly exceeds this limit but remains acceptable for supervisory applications and corrective actions within a few cycles. By contrast, the VSAT link induces latencies around 650 ms, which are incompatible with instantaneous triggering but suitable for deferred supervision and redundancy. Therefore, only the fiber link guarantees strict IEC conformity, while 4G and VSAT must be interpreted as complementary channels with operational constraints.

These performances align with the findings of [20] and [21], which emphasize the ability of neuro-fuzzy systems to combine rapid reaction with noise tolerance.

The ablation experiments (Tables 4 and Table 5) show that QoS modulation of the membership functions enhances ANFIS decision stability, particularly on channels subject to jitter and loss such as 4G and VSAT. These results extend the work of [22]-[24] on integrating communication metrics into diagnostic algorithms, but apply them for the first time to a near real-time ANFIS system tailored to an African grid. Thus, the proposed architecture goes beyond classical approaches where QoS is considered exogenous.

Sliding RMS threshold approaches, in line with standards such as EN 50160 and IEC 61000-4-30, remain benchmarks for power quality monitoring. However,

they suffer from high sensitivity to noise and a latency induced by window size, which limits their responsiveness in unstable environments. Frequency-domain methods (FFT, DFT) or wavelets [25] [26] offer better spectral resolution and improved detection of non-stationary disturbances, but their deployment in constrained grids such as Congo-Brazzaville is hindered by computational cost and sensitivity to frequency variability.

The proposed ANFIS approach combines the interpretability of fuzzy logic with neural adaptability, making it a robust and contextually suitable alternative for hybrid and heterogeneous environments. Our results (**Tables 6** and **Table 7**) outperform ANN and RMS baselines by 46 macro-accuracy points, confirming the observations of Bilgundi *et al.* [27], while adding the critical dimension of hybrid transmission (Fiber, 4G, VSAT), absent from prior work.

Unlike earlier studies conducted on interconnected European or Asian grids, this work explicitly incorporates the communication constraints of the Congolese context: limited fiber coverage, unstable mobile networks, and high VSAT latency. The QoS-based routing scheme (**Figure 4**) and automatic failover logic provide an original response, experimentally validated by the resilience of ANFIS diagnostics under varying QoS conditions. The hybrid transmission scheme relies on priority routing with hysteresis-based failover. Critical flows are preferentially assigned to the fiber link, while 4G/LTE is used as a backup or for semi-critical traffic. VSAT remains a last resort option to guarantee minimal connectivity in remote areas. Bandwidth allocation follows a hierarchical policy: critical diagnostic packets are prioritized, while non-critical logs are deferred to lower-quality links. From a cost-performance perspective, fiber ensures the lowest latency but requires heavy infrastructure investment, 4G/LTE provides flexibility at moderate cost but suffers from congestion, and VSAT offers universal coverage at the expense of high latency and recurring service fees. This trade off analysis highlights that hybridization balances performance with economic and geographical constraints. This contribution paves the way for an adaptation of African smart grids where robustness takes precedence over raw performance.

In summary, this study demonstrates that coupling **ANFIS + hybrid transmission** is a robust, context-aware, and scientifically grounded approach for detecting sags/swells in African HV networks. It reinforces the relevance of neuro-fuzzy approaches in the literature while contributing an original dimension linked to the heterogeneity of communication channels in constrained contexts.

9. Conclusions

This study has demonstrated that a diagnostic system based on a neuro-fuzzy ANFIS model, coupled with a hybrid telecommunication architecture integrating fiber optic, 4G/LTE, and VSAT, provides an effective response to the supervision challenges of Congolese high-voltage networks. The results highlight the superiority of ANFIS over classical approaches, both in terms of sag/swell classification accuracy and detection speed, while maintaining high performance even under

degraded QoS conditions. This robustness stems in particular from the explicit integration of communication metrics into the fuzzy premises, which grants the system unprecedented decision stability in heterogeneous environments.

Beyond experimental validation, this research makes an original contribution to the literature by proposing a novel articulation between artificial intelligence and the resilience of transmission channels, thus opening a credible pathway for the modernization of African power grids.

Despite the performances obtained on real data from the Congolese network, certain limitations remain and open avenues for further research. The high latency of VSAT (650 ms, Table 3) is still incompatible with instantaneous triggering, restricting this link to deferred supervision. Moreover, multi-event scenarios (e.g., a sag occurring simultaneously with a swell or harmonics) require an enrichment of the ANFIS rule base with time-scale indices, notably through the use of multi-scale wavelets. Building on this work, future perspectives include the implementation of field prototypes to confront the system with real perturbations in a full operational context, the extension of diagnostics to other power quality indicators such as harmonics or flicker, and the integration of synchronized measurement devices (PMU, μPMU). These developments will enhance fault localization, strengthen interoperability with international standards, and ensure the transferability of the ANFIS model to other African grids facing similar constraints.

In conclusion, this study confirms that combining an ANFIS system with hybrid transmission is not only a high-performance technical solution, but also a structuring step toward smarter, more resilient grids that are better adapted to the realities of African infrastructures.

Acknowledgements

The authors gratefully acknowledge the **Supelec** (supelec.engineering@gmail.com) and **Matelek** (matelekingenierie@gmail.com) laboratories for their insightful discussions, technical assistance, access to computing resources, and valuable feedback throughout this work.

Conflicts of Interest

The authors declare no conflicts of interest.

References

[1] Singh, B., Chandra, A. and Al-Haddad, K. (2015) Power Quality: Problems and Mitigation Techniques. John Wiley & Sons.

[2] ISCC P Quality (1995) IEEE Recommended Practice for Monitoring Electric Power Quality.

[3] Moravej, Z., Abdoos, A.A. and Pazoki, M. (2009) Detection and Classification of Power Quality Disturbances Using Wavelet Transform and Support Vector Machines. *Electric Power Components and Systems*, **38**, 182-196. https://doi.org/10.1080/15325000903273387

[4] Nianga-Apila, Gogom, M., Ganongo, A.O., Gomba, R. and Ganga, G. (2025) Detecting and Locating Short-Circuit Faults in Electrical Mesh Networks. *Energy and Power Engineering*, **17**, 134-153. https://doi.org/10.4236/epe.2025.176007

[5] Ganongo, A.O., Gogom, M., Nianga-Apila, Obita, L.L.A. and Ganga, G. (2024) Optimisation of Lightning Current Discharge to the Ground in Electrical Networks: Introduction of the Proportionality Coefficient (K). *Electric Power Systems Research*, **231**, Article ID: 110348. https://doi.org/10.1016/j.epsr.2024.110348

[6] Gogom, M., Tsahat Oboulhas, C.O., Apila, N., Oko Ganongo, A. and Lilonga-Boyenga, D. (2022) Optimization of Losses Joule in the Congolese Electrical Network Integrated with the Energy Pool of Central Africa in the PEAC Acronym. *Energy and Power Engineering*, **14**, 13-34. https://doi.org/10.4236/epe.2022.141002

[7] Ngouloubi, T., Gomba, R., Gogom, M., Nianga-Apila, M. and Eyandzi, A. (2025) Optimization of a Medium-Voltage Distribution Network via Photovoltaic Integration: A Case Study of the Liouesso MT Grid. *Science Journal of Energy Engineering*, **13**, 108-119. https://doi.org/10.11648/j.sjee.20251303.11

[8] Calderon Mendoza, E.M. (2018) Méthodes de localisation et de détection de dé-fauts d'arcs électriques séries dans un réseau électrique alternatif basse tension. Ph.D. Thesis, Universite de Lorraine.

[9] Bouguila, Z.*I.E.*D., Moukadem, A., Abdeslam, D.O., Wira, P. & Dieterlen, A. (2013) Nouvelle méthode de détection des perturbations dans les signaux électriques basée sur la transformée de Stockwell. *XXIVe Colloque GRETSI*, Brest, September 2013, 3-6.

[10] Caujolle, M. (2011) Identification et caractérisation des perturbations affectant les réseaux électriques HTA. Supélec.

[11] Barazane, L. (2007) Optimization par un contrôleur anfis des performances d'une nouvelle approche de modelisation floue du moteur asynchrone. 4*th International Conference on Computer Integrated Manufacturing CIP*'2007, Sétif, 3-4 November 2007.

[12] Gouriveau, R., El Koujok, M. and Zerhouni, N. (2007) Spécification d'un système neuro-flou de prédiction de défaillances à moyen terme. *Rencontres Francophones sur la Logique Floue et ses Applications*, *LFA*'2007, Nîmes, 22-23 Novemer 2007, 65-72.

[13] Bendary, A.F., Abdelaziz, A.Y., Ismail, M.M., Mahmoud, K., Lehtonen, M. and Darwish, M.M.F. (2021) Proposed ANFIS Based Approach for Fault Tracking, Detection, Clearing and Rearrangement for Photovoltaic System. *Sensors*, **21**, Article 2269. https://doi.org/10.3390/s21072269

[14] Zhu, X. and Jiang, C. (2022) Integrated Satellite-Terrestrial Networks toward 6G: Architectures, Applications, and Challenges. *IEEE Internet of Things Journal*, **9**, 437-461. https://doi.org/10.1109/jiot.2021.3126825

[15] Tezergil, B. and Onur, E. (2022) Wireless Backhaul in 5G and Beyond: Issues, Challenges and Opportunities. *IEEE Communications Surveys & Tutorials*, **24**, 2579-2632. https://doi.org/10.1109/comst.2022.3203578

[16] Abrahamsen, F.E., Ai, Y. and Cheffena, M. (2021) Communication Technologies for Smart Grid: A Comprehensive Survey. *Sensors*, **21**, Article 8087. https://doi.org/10.3390/s21238087

[17] Artiga, X. and Pérez-Neira, A.I. (2015) Shared Access Terrestrial-Satellite Backhaul Network Enabled by Smart Antennas: Sansa. *Proceeding of European Conference Networks Communications*, Paris, 29 June-2 July 2015, 46-53.

[18] Kuzlu, M., Pipattanasomporn, M. and Rahman, S. (2014) Communication Network

Requirements for Major Smart Grid Applications in HAN, NAN and Wan. *Computer Networks*, **67**, 74-88. https://doi.org/10.1016/j.comnet.2014.03.029

[19] Deng, C., Xiao, X., Fu, Z., Liu, G., Yang, H. and Liu, J. (2011) Terrestrial-Satellite Hybrid Backbone Communication Network for Smart Power Grid. *Energy Procedia*, **12**, 27-36. https://doi.org/10.1016/j.egypro.2011.10.006

[20] Syahrin, A.A., Anggriawan, D.O., *et al.* (2023) Real-Time Detection of Power Quality Disturbance Using Fast Fourier Transform and Adaptive Neuro-Fuzzy Inference System. *Jurnal Rekayasa Elektrika*, **19**, 12-19.

[21] Chapala, S., R. L, N. and Das. G, T.R. (2024) Power Quality Analysis of ANFIS Based-distributed Generation System with UPQC. *International Journal of Engineering and Manufacturing*, **14**, 1-14. https://doi.org/10.5815/ijem.2024.04.01

[22] Folorunsho, S.O., Adenekan, O.A., Ezeigweneme, C., Somadina, I.C. and Okeleke, P.A. (2024) Optimizing Network Performance and Quality of Service with AI-Driven Solutions for Future Telecommunications. *International Journal of Frontiers in Engineering and Technology Research*, **7**, 73-92. https://doi.org/10.53294/ijfetr.2024.7.1.0041

[23] Duvvuri, S.K. and Ramakrishna, S. (2021) Adaptive Neuro-Fuzzy Inference System Based On-Demand Fault Tolerant Routing Protocol (ANFIS-ODFTR) for Manets. *International Journal of Computer Networks and Applications*, **8**, 719-729. https://doi.org/10.22247/ijcna/2021/210721

[24] Shah, G.A., Gungor, V.C. and Akan, (2013) A Cross-Layer QOS-Aware Communication Framework in Cognitive Radio Sensor Networks for Smart Grid Applications. *IEEE Transactions on Industrial Informatics*, **9**, 1477-1485. https://doi.org/10.1109/tii.2013.2242083

[25] Molu, R.J.J., Mbasso, W.F., Saatong, K.T., Dzonde Naoussi, S.R., Alruwaili, M., Elrashidi, A., *et al.* (2024) Enhancing Power Quality Monitoring with Discrete Wavelet Transform and Extreme Learning Machine: A Dual-Stage Pattern Recognition Approach. *Frontiers in Energy Research*, **12**, Article 1435704. https://doi.org/10.3389/fenrg.2024.1435704

[26] Gupta, S. and Sharma, A.K. (2015) Power Quality Identification Using Wavelet Transform: A Review. *International Journal of Recent Research in Electrical and Electronics Engineering*, **2**, 42-48.

[27] Bilgundi, S.K., Sachin, R., Pradeepa, H., Nagesh, H.B. and Likith Kumar, M.V. (2022) Grid Power Quality Enhancement Using an ANFIS Optimized PI Controller for DG. *Protection and Control of Modern Power Systems*, **7**, Article No. 3. https://doi.org/10.1186/s41601-022-00225-2

Appendix A: Transmission Budget and Technology Selection for ANFIS Systems

To size the telecommunication chain, we distinguish between the raw data rate (all samples) and the effective data rate after local preprocessing (RTU). Table A1 summarizes the calculation and the orders of magnitude considered for ANFIS.

Table A1. Data rate budget per measurement site for ANFIS input.

Scenario	Assumptions/Formula	Estimated rate
Raw transmission	$N = 6$ channels (3 voltages + 3 currents), $f_s = 20$ kHz, $Q = 16$ bits	
$D = N \cdot f_s \cdot Q$	$6 \times 20000 \times 16 = 1.92$ Mbit/s	
After *RTU preprocessing* (RMS/FFT/features)	Feature and/or event extraction (50 Hz windows)	**20-200 kbit/s** (typical)
Protocol overhead (headers, VPN)	Conservative upper bound ≈ +20% applied to useful rate	× 1.2
Dimensioning rate (critical flows)	Conservative example: 200 kbit/s×1.2	**240 kbit/s**

We compare fiber, 4G/LTE, and VSAT in terms of latency, jitter, loss, useful throughput, and availability. Table A2 positions each technology with respect to ANFIS requirements.

Table A2. Comparison of transmission technologies for supplying an ANFIS diagnostic system.

Technology	Latency	Jitter	Loss	Useful rate	Avail.	ANFIS suitability
	(ms)	(ms)	(%)	(kbit/s)	(%)	(recommended usage)
Fiber optic	<5	<1	<0.1	>10^6	>99.9	Critical flows (quasi real-time)
G/LTE	30-70	5-30	0.1-2.0	500-10,000	95-99	Continuity/redundancy (P=2)
VSAT (GEO)	500-900	20-60	0.5-2.0	64-512	98-99.5	Deferred supervision/backup

Note: Weather degrades VSAT (rain/storm). Fiber and 4G data rates largely exceed the dimensioning rate (Table A1).

Appendix B: Data on the Congolese Electricity Network

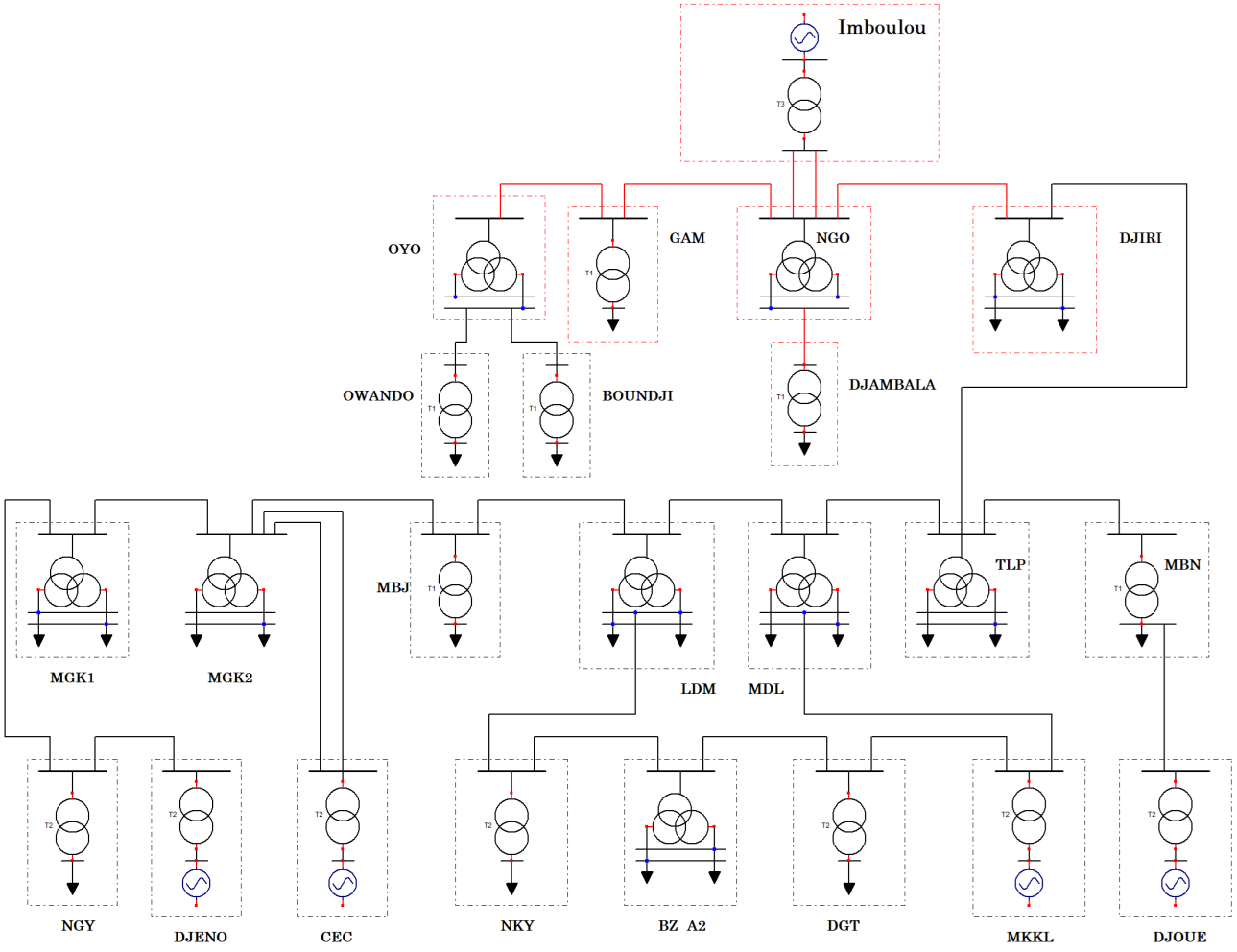

Figure S1. Congolese network.

Table B1. Transformer Characteristics.

2*—	Voltage (kV)			Resistance (p.u.)			Inductance (p.u.)		
	Primary	Secondary	Tertiary	Primary	Secondary	Tertiary	Primary	Secondary	Tertiary
T1	10.5	220	—	0.0080606	0.0102313	—	0.35115575	0.351101	—
T2	220	110	30	0.0105	0.0133333	0.0288889	0.4345398	0.4344621	0.8688532
T3	220	30	—	0.0335	0.042	—	1.3025693	1.3023229	—
T4	220	110	30	0.0070429	0.0070925	0.0088814	0.4352764	0.4352755	0.4352427
T5	220	110	30	0.05	0.084	0.06	2.6055203	2.1983958	1.3987137
T6	110	30	—	0.04756	0.03876	—	1.0789523	1.0793042	—

Table B2. Node powers in p.u. with losses (2%).

Node	P_G (p.u.)	Q_G (p.u.)	P_{Ch} (p.u.)	Q_{Ch} (p.u.)
Imboulou (Generator)	1.2000	0.7423	0.0129	0.0059

Continued

Network losses (2%)	–	–	0.0240	0.014846
Djiri	–	–	1.0877	0.699254
Ngo	–	–	0.0027	0.0013
Djambala	–	–	0.0117	0.0035
Gamboma	–	–	0.0105	0.0023
Oyo	–	–	0.0505	0.0152

Table B3. Line parameters and transmission capacities.

Lines/Sections	Length (km)	Voltage (kV)	Resistance (p.u./Ω)	Reactance (p.u./Ω)	Susceptance
IMB-Ngo (2-3(×2))	77	220	0.015	0.067	0.0507
Ngo-Djiri (3-4)	207.87	220	0.024	0.173	0.142
Ngo-Gamboma (3-7)	75.2	220	0.009	0.063	0.0516
Gamboma-Oyo (7-9)	87.6	220	0.010	0.073	0.0602
Ngo-Djambala (13-14)	109	110	0.117	0.333	0.019

Appendix C: Functional Architecture of the System for PQ Detection

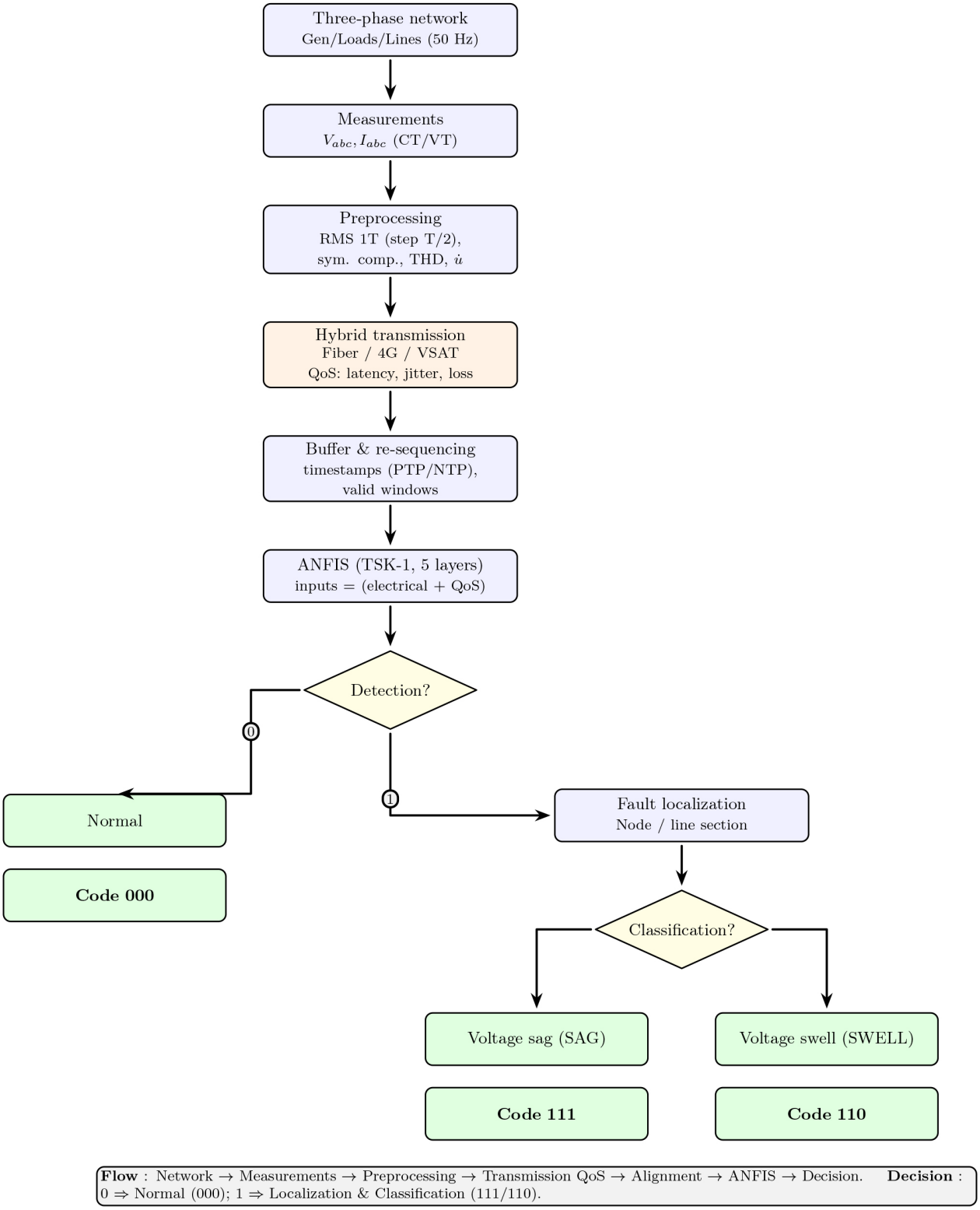

Figure S2. PQ detection chain (SAG/SWELL) with ANFIS and hybrid QoS-based transmission.